Heliyon 5 (2019) e01792

Contents lists available at ScienceDirect

Heliyon

journal homepage: www.heliyon.com

Heliyon

An evaluation of subcritical hydrothermal treatment of end-of-pipe palm oil mill effluent

Zhan Sheng Lee, Sim Yee Chin, Chin Kui Cheng *

Faculty of Chemical and Natural Resources Engineering, Universiti Malaysia Pahang, Lebuhraya Tun Razak, 26300, Gambang, Kuantan Pahang, Malaysia

ARTICLE INFO

Keywords:
Environmental science
Chemical engineering

ABSTRACT

This study evaluates the effects of subcritical hydrothermal treatment on palm oil mill effluent (POME) and its concomitant formations of solid hydrochar, liquid product and gaseous product. The reactions were carried out at temperatures ranged 493 K–533 K for 2 h. The highest reduction of chemical oxygen demand (COD) and biochemical oxygen demand (BOD) were 58.8% and 62.5%, respectively, at 533 K. In addition, the removal of total suspended solids (TSS) achieved up to 99%, with the pH of POME reaching 6 from the initial pH 4. The gas chromatography coupled with mass spectroscopy (GC-MS) analysis showed that the fresh POME contained n-Hexadecanoic acid as the dominant component, which gradually reduced in the liquid product in the reaction with increased temperature, in addition to the attenuation of carboxyl compounds and elevation of phenolic components. The gaseous products contained CO_2, CO, H_2, and $C_3 - C_6$ hydrocarbons. Traces of CH_4 were only found at 533 K. CO_2 is the dominant species, where the highest of 3.99 vol% per 500 mL working volume of POME recorded at 533 K. The solid hydrochars showed negligible morphological changes across the reaction temperature. The O/C atomic ratio of the hydrochar range from 0.157 to 0.379, while the H/C atomic ratio was in the range from 0.930 to 1.506. With the increase of treatment temperature, the higher heating value (HHV) of the hydrochar improved from 24.624 to 27.513 MJ kg^{-1}. The characteristics of hydrochar make it a fuel source with immense potential. POME decomposed into water-soluble compounds, followed by deoxygenation (dehydration and decarboxylation) in producing hydrochar with lower oxygen content and higher aromatic compounds in the liquid product. Little gaseous hydrocarbons were produced due to subcritical hydrothermal gasification at low temperature.

1. Introduction

Agriculture sector in Malaysia has contributed 8.1%, worth RM 89.5 billion, to the Gross Domestic Product (GDP) in the year 2016 (DOSM, 2017). Oil palm sector is the main contributor with 43.1% of the GDP of agriculture sector (DOSM, 2017). The continuous growth in palm oil production and export has catapulted Malaysia to the second ranking of crude oil producer after Indonesia (Foong et al., 2018). The main exported palm oil related products are oleochemicals, palm oil, biodiesel, palm kernel oil (PKO), palm kernel cake (PKC) and finished products that are valued at more than RM74 million in 2017 (MPOB, 2017).

During the palm oil processing, one tonne of crude palm oil (CPO) can be produced from 5 tonnes of fresh fruit bunches (FFB). Significantly, the processing of each tonne of FFB produces 0.65–0.67 tonne of POME (Stichnothe and Schuchardt, 2011). Each tonne of POME generates 28 m^3 of CH_4, an anthropogenic greenhouse gas in the atmosphere besides the CO_2 (Olivier et al., 2009). POME physically appears as thick and brownish viscous liquid waste (Hosseini and Wahid, 2015; Wu et al., 2010). It has biological oxygen demand (BOD) that range from 25000 to 35000 mg/L and an average chemical oxygen demand (COD) of 54000 mg/L. Moreover, it is acidic with a pH of 4.5 due to the presence of organic acids (Tabassum et al., 2015). Improper treatment and discharge of POME can cause negative impact to the aquatic system owing to its high COD and BOD levels.

POME is not a single-source wastewater but consists of a combination of wastewater from three main sources, *viz*. clarification (60%), sterilisation (34%) and hydrocyclone (6%) (Ahmad and Ghufran, 2018). POME contains various suspended constituents, namely cell walls, short fibres, organelles, a series of carbohydrates ranging from hemicellulose to simple sugars, various nitrogenous compounds from proteins to amino acids, free organic acids, and an assembly of minor organic and mineral components (Ahmad and Ghufran, 2018; Wu et al., 2010).

* Corresponding author.
E-mail address: chinkui@ump.edu.my (C.K. Cheng).

https://doi.org/10.1016/j.heliyon.2019.e01792
Received 7 January 2019; Received in revised form 25 March 2019; Accepted 20 May 2019

Environmental Quality Act 1974 regulates the effluent disposal from the palm oil industry. Malaysia's Department of Environmental (DoE) has enforced a comprehensive wastewater discharge policy; the BOD value of POME must be reduced to 100 ppm threshold. Since 2006, 20 ppm BOD discharge limit has been enforced in East Malaysia (MPOA, 2014). However, there is no regulatory control for both COD and total solids (TS) from DoE after 1984, for POME discharge.

In spite of strict regulations, it can be difficult to meet the discharge criteria, which can be attributed to obsolete waste treatment system (Ng and Cheng, 2016). More than 85% of the oil palm millers employ open ponding system for POME treatment as this method is relatively cheap and incurs low operating cost (Poh and Chong, 2009). Nevertheless, this treatment system suffers from long hydraulic retention time (HRT), typically around 45–60 days, vast land area for pond creation, terrible odour and difficulty in sustaining liquor distribution and biogas collection (Zinatizadeh et al., 2006).

Over the years, numerous alternate POME treatment methods to overcome the drawbacks of current system have been evaluated. Methods such as coagulation-flocculation (Zahrim et al., 2017; Teh et al., 2016), microbial fuel cell (Cheng et al., 2010), up-flow anaerobic sludge blanket – hollow centred packed bed (UASB-HCPB) (Chan et al., 2015; Poh and Chong, 2014), membrane filtration (Ali et al., 2015), advanced oxidation processes (AOP) (Alhaji et al., 2018; Ng et al., 2016; Ng and Cheng, 2015) and ultrasonic-assisted membrane anaerobic system (USMA) (Jamal et al., 2007) were reported. Nevertheless, these systems have limited scale up potential, mainly due to both capital and operating cost. In addition, most of the studies were only conducted at laboratory-scale, far from industrial practicality.

Recently, the conversion of wet biomass into useful hydrochar, bio-oil and gaseous products using pressurised hydrothermal process has gained a lot of interest due to its perceived “green pathway”. Hydrochar is a carbon-rich solid residue product generated from the hydrothermal treatment. Extensive studies have been done on hydrochar production from different biomass, such as wood chips, empty fruit bunches, microalgae, pine and fruit wastes (Zhang et al., 2018; Simsir et al., 2017; Wu et al., 2017; Parshetti et al., 2013; Heilmann et al., 2010). Hydrochar as an intermediate product that can be further processed into some value-added substance, such as a low-cost adsorbent (Islam et al., 2017; Takaya et al., 2016), solid fuels (Liu et al., 2014; Liu et al., 2013), supercapacitors (Gao et al., 2015; Ding et al., 2013) and for carbon sequestration as well as soil amendment (Windeatt et al., 2014; Tsai et al., 2012; Sevilla and Fuertes, 2009).

From our search in the literature, hydrothermal treatment of POME in subcritical condition remains unexplored. Subcritical water is a state in the temperature range of 373–647 K and the pressure in the system must be at or above saturated pressure to ensure the water remains as liquid (Kruse et al., 2013; Cheng et al., 2009). Subcritical hydrothermal treatment possesses several benefits as it is easy to implement, and has low capital and operational costs (Abu Tayeh et al., 2016), due to low temperature requirement (Osada et al., 2004).

In comparison to the open ponding system, hydrothermal process could treat POME in a substantially reduced reaction time without requiring large area of land, while producing value-added products as the treatment output. Besides, hydrothermal process is more energy-saving compared to conventional bioenergy production, because the organic-rich wastewater such as POME can be converted to useful products without prior-drying. To the best of our knowledge, no systematic study has been done on investigating the products from POME hydrothermal treatment. Thus, pressurised subcritical hydrothermal treatment of POME was carried out in the current work to evaluate the process. The effects of reaction temperature on the wastewater quality treatment and its concomitant product distribution was investigated.

2. Materials and methods

2.1. Feedstock collection and storage

30-L of fresh POME was collected from a local palm oil mill based in Gambang, Kuantan. The collection point was at the end-of-pipe and was not pre-treated to preserve the originality. The temperature of the effluent was measured directly using a thermometer. It was characterised on the same day to obtain the initial properties. The POME was then tightly-sealed in a black container and kept in the fridge at temperature of 277 K. Prior to the hydrothermal subcritical treatment, the POME in the container was gently shaken to ensure its homogeneity.

2.2. Subcritical hydrothermal treatment of POME

The reactor was operated in a batch mode from 493 K to 533 K for 2 h. The liquor was stirred at a single speed of 500 rpm. A working volume of 500 mL was used in all subcritical, highly-pressurised hydrothermal reaction. Inert N_2 gas was channelled into the reactor for purging, prior to each experiment. Initial pressure in the reactor was set at 50 bar, followed by an autogenous pressure built up throughout the reaction to maintain the POME at liquid phase. In the heating phase, 30 min–40 min were required to achieve the set point temperature. The temperature remained constant for 2 h during the holding phase, where the high pressure hydrothermal process occurred. To ensure the reproducibility of the reaction, all the experiments were run in triplicates. Sampling of gas product was done after the 2 h reaction. For the liquid product, it was discharged into a 500-mL beaker from a drain valve located at the bottom of the reactor. The liquid sample was subsequently stored in sampling bottles for further analysis. The wet hydrochar was collected using a spatula by removing it from the inner wall of reactor and magnetic stirrer. The wet hydrochar was then oven-dried at 378 K for 3 h to remove the physically-bound moisture, prior to further analyses.

2.3. Liquid product analysis

Liquid samples from different runs were selectively chosen for analyses of their wastewater qualities, such as pH, chemical oxygen demand (COD), biological oxygen demand (BOD) and total suspended solids (TSS). The pH value of POME was determined using pH indicator strips, sourced from Merck. For COD analysis, a total 2 mL of diluted POME sample was pipetted into the oxidation vial. Meanwhile, a vial with distilled water was used as the datum. The vials were then placed in the vial socket of DRB200 reactor followed by heating to 423 K and maintained at the stipulated temperature for 2 h. The reading of each vial was repeated for three times. In addition, BOD for 5 days (BOD_5) was measured to determine the oxygen uptake by the microorganisms in the samples. A total of 1 mL for each of the phosphate buffer, magnesium sulphate ($MgSO_4$), calcium chloride ($CaCl_2$), ferric chloride ($FeCl_3$) solutions were mixed and diluted to a 1000 mL dilution water. The fresh POME and liquid products were diluted at dilution factors of 1500 and 100, respectively, using the dilution water. The prepared samples were transferred to 300 mL incubation bottle, with drop-wise addition of 1 N NaOH to maintain the pH in the range of 6.5–7.5. The incubation bottles were stored in a BOD incubator at 293 K for 5 days after measuring the initial DO. The BOD_5 readings were obtained using Eq. (1).

$$BOD_5\ (ppm) = (D_i - D_f)/P \quad (1)$$

where D_i, D_f and P represent the initial DO value, final DO value and decimal volumetric fraction of sample used, respectively.

TSS of POME was checked using vacuum filtration through a 47-mm nylon membrane with a pore size of 0.45 μm. 100 mL of diluted POME sample was filtered through the membrane, which was washed and dried to a constant weight. After the filtration process, the membrane was dried repeatedly at 323 K until a constant weight obtained. The TSS in mg/L

was calculated based on the weight difference of the membrane.

The fresh POME and liquid stream were subjected to freeze-drying process to obtain the residues for gas chromatography coupled with mass spectroscopy (GC-MS) analysis. The freeze-drying process was done by subjecting 50 mL of each sample into Labconco freeze dryer at 193 K and 0.14 mbar. The freeze-dried sample was then fed to Agilent 7890A GC-MS with thermal desorption system to identify the organic components in the POME sample. The freeze-dried sample powder was loaded on a micro-vial before inserting to the GC injector, where the available compounds were eluted by 1 mL/min of He gas through a capillary column, *viz.* Agilent J&W DB 5-ms (30 m × 0.25 mm ID, 0.25 μm df, Fused Silica). A ramping rate of 8 K/min was employed to raise the initial temperature of GC column from 323 K to 473 K, followed by ramping rate of 10 K/min to 573 K. The GC oven was operated at 573 K while the injector port and MS detector were operated at 523 K. NIST mass spectral library was available for identification of compounds.

2.4. Gaseous product analysis

Gas sampling bags were used to collect the gaseous product before it was injected to a gas chromatography (GC) instrument to determine the composition of gas. The GC-Agilent 6890 N series was equipped with TCD and two packed columns; Supelco Molecular Sieve 13× (10 ft × 1/8 in OD × 2 mm ID, 60/80 mesh, stainless steel) and Agilent Hayesep DB (30 ft × 1/8 in OD × 2 mm ID, 100/120 mesh, stainless steel) for detecting CO_2, CH_4, H_2 and CO. Helium was used as a carrier gas with effective column temperature of 393 K and flowrate of 20 mL/min. A full separation of the gas components required a retention time of around 15 min.

2.5. Solid product analysis

The percentages of fixed carbon (FC), volatile matter (VM) and ash are commonly measured via thermogravimetric analysis (TGA) for quality characterisation of fuel materials and their thermal properties (Stirling et al., 2018; Zhao et al., 2016). The hydrochars were dried in oven at 378 K for 24 h to remove the moisture content prior to dry-basis TGA work. In this work, the thermogravimetric profile of 6.5 mg hydrochar on an aluminium pan was conducted using Hitachi STA7000. The temperature was ramped from 303 K to 623 K under 50 mL/min of N_2 flow, followed by 50 mL/min air flow up to 1273 K, at a heating rate of 5 K/min. At the end of the analysis, the sample was held at 1273 K for 15 min to determine the ash content. The FC percentage in weight was calculated based on Eq. (2).

$$\text{FC}\ (\%) = 100 - \text{VM}\ (\%) - \text{Ash}\ (\%) \quad (2)$$

The high heating value (HHV) of the hydrochar was estimated using Channiwala and Parikh formula (Channiwala and Parikh, 2002) shown in Eq. (3), which is typically employed for its acceptable accuracy, where 1.45% and 0.00% for average absolute error and bias error, respectively. All the spectrum of the hydrochar consisting of gas, liquid and solid phase would be included entirely in the formula as well (Zhang et al., 2015).

$$\text{HHV}\ (\text{MJ/kg}) = 0.3491\text{C} + 1.1783\text{H} + 0.1005\text{S} - 0.1034\text{O} - 0.0151\text{N} - 0.021\text{A} \quad (3)$$

where, C, H, S, O, N and A represent elements of carbon, hydrogen, sulphur, oxygen, nitrogen and ash content in weight percentage (wt %), in sequence.

The elemental analysis on dry basis of hydrochar for C, H, S and N contents was performed using Perkin Elmer Series II CHNS/O Analyser 2400 and the elemental O content was determined by difference.

The surface morphology of hydrochar samples was analysed using SEM-EDX (Brand: FEI Quanta 450). The integrated EDX detector was utilised to study the elemental distribution on the samples surface. FEI software was used in interpreting and quantifying data. For the sample preparation, the hydrochar was oven-dried at 378 K for 24 h to evaporate the moisture content. 50 mg of dried samples were cut with a razor blade in the desired shape before it was evenly dispersed onto a carbon conductive pad on top of an aluminium stub. The prepared samples were then coated with Pt to minimise the charging effect. The stubs were placed on the sample rack in the specimen chamber of the microscope. Images of the hydrochar were generated by using an electron beam of 10 kV with a spot size of 4. High vacuum mode was prioritised in the SEM imaging with sputter coating done on the samples surface to get the best images.

3. Results & discussion

3.1. Liquid phase analysis

3.1.1. Fresh POME characterisation

Table 1 shows the comparison between properties of fresh POME used in the current study and the published data in literature. For the present study, all the characteristics of collected POME were in the range of POME as previously reported (Ng et al., 2018; Nasrullah et al., 2017; Tabassum et al., 2015).

3.1.2. Liquid product characterisation

Characterisation of POME post-treatment showed an overall reduction in COD, BOD_5 and TSS, as well as an increase in pH value. The pH values for all samples are acidic as shown in Fig. 1. It may be attributed to the remaining organic acids in the products that was originated from the decomposition of monosaccharides content in fresh POME (Berge et al., 2011). The pH values were higher in all the liquid products and showed a consistent increase from 493 K to 533 K, as shown in Fig. 1. As indicated by the GC-MS analysis results in Table 2, the carboxylic compounds in the fresh POME probably has transformed into a carbon-densified hydrochar and gases such as CO_2 and CO with the increase of reaction temperature. The step-up of phenolic compounds was derived from the slow degradation of lignin in POME at the increase of reaction temperature.

Fig. 2 shows that both COD and BOD_5 reduction gradually increased with the increase of hydrothermal temperature. The COD and BOD_5 readings at 493 K were 36400 ppm and 9178 ppm, respectively, while the COD reading recorded 21500 ppm and 7477 ppm for the BOD_5 reading at 533 K. The liquid product achieved a COD reduction of 30.3% and 58.8% at 493 K and 533 K respectively. Meanwhile, highest BOD_5 reduction also recorded at 533 K, which has a value of 67.6%, compared to the lowest of 35.6% at 493 K. Compared to the open ponding system, these results are remarkable, assuming a 2 h hydrothermal treatment in the commercial-scale batch reactor is with proper design that could minimise the limitation of mixing, mass and heat transfer to maintain the lab-scale performance (Coker, 2001).

Fig. 2 also displays a TSS reduction of more than 90% in all experiment sets. TSS reduction showed a gradual increase from 493 K to 533 K, equivalent to reductions of 90.12% and 99.42%, respectively. The improving reduction percentage could be due to the increased amount of hydrochar which was readily separable from the liquid product.

Table 1
Comparison of fresh POME properties.

Properties[a]	General Range (Ng et al., 2018; Nasrullah et al., 2017; Tabassum et al., 2015)	Present study
pH	3.6–4.3	4.0
COD	25,000–75,000	52,200
BOD_5	15,600–27,000	19,920
TSS	20,000–50,000	34,800
Temperature (K)	353–363	360

[a] The units are in mg/L, except for pH and temperature.

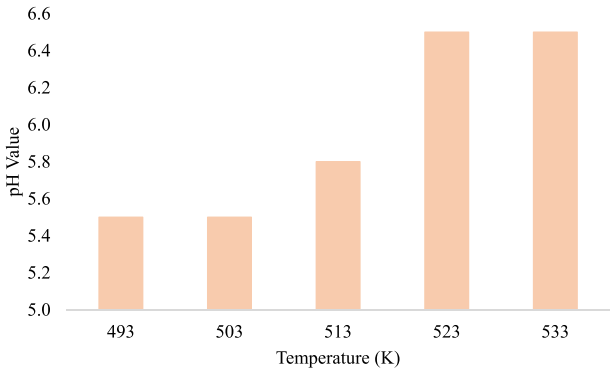

Fig. 1. pH value of the liquid output.

3.1.3. GC-MS analysis

The GC-MS spectra of freeze-dried fresh POME and liquid products after hydrothermal reaction of POME are recorded in Fig. 3(a) , (b), (c), (d), (e), (f). The result shows that n-hexadecanoic acid, which commonly known as palmitic acid, is the most abundant organic compound in the fresh POME, followed by 1,1-dimethyl-hydrazine, allyl ethyl ether and some traces of organic components which can be regarded as negligible. Palmitic acid constitutes the major organic component of POME, consistent with natural content of palm oil (Montoya et al., 2014). These dominant organic compounds found were in agreement with the findings of other researchers (Cheng et al., 2010, 2018).

A total of 19 organic compounds were found in the fresh POME. Nonetheless, a total of 87 organic components were detected in hydro-treated POME at 493 K. It can be inferred that the organic constituents hydrolysed into simpler components. Significantly, these numbers decreased further to 35, 40, 26 and 26 types of reaction products at 503 K, 513 K, 523 K and 533 K, respectively. Long-chain organic compounds comprised primarily carboxylic and phenolic compounds were found in the liquid phase. The concentration of carboxyl compounds decreased gradually with the increase of reaction temperature, while the phenolic group compounds increased in accordance to the rise of temperature, as shown in Fig. 4.

In addition to the phenolic compounds, minor compounds of ketones, aldehydes, alkene and amine were detected. Some of the alcohols started to appear at 533 K, including 1-(1-propynyl)cyclohexanol, 2,2-dimethyl-1-pentanol and O-Methoxy-.alpha.-methylbenzyl alcohol. This suggests us the slow growth of phenolic compounds in the liquid products as more alcohols were detected at higher temperature. The possible degradation pathways of all these compounds could be deoxygenation at lower temperature and subcritical hydrothermal gasification at higher temperature. The degradation mechanism of all the intermediate organic components could be further investigated using other approaches.

3.2. Gaseous product analysis

The gas produced from the subcritical hydrothermal treatment of POME for 2 h in various temperature was also analysed. The gaseous products mainly comprised of CO_2, CO, H_2 and traces of higher number carbon gases (C_3 – C_6). Traces of CH_4 were observed at 533 K as it can only be produced at higher temperature through CO methanation. The gas composition at different reaction temperatures is depicted in Fig. 5. The dominant gas product was CO_2, where the lowest of 3.10 vol% at 493 K while the highest of 3.99 vol% per working volume of 500 mL POME at 533 K. By ignoring CH_4, the H_2 production was the smallest, which in the range of 0.0005–0.03 vol% over 500 mL POME. The insignificant production of H_2 could be possibly due to two main reasons. Firstly, POME contains higher lignin-to-cellulose ratio compared to the other agricultural fibrous residues (Wong et al., 2008). Biomass with higher composition of cellulose and hemicellulose would produce more H_2, while H_2 yield will be inhibited by the existence of lignin in the structure of biomass (Salimi et al., 2016). Another reason for the low volume of H_2 generated was due to the absence of catalyst in this range of temperature. The catalyst is suggested to aid in turning the big molecules into smaller molecules on the catalyst surface, followed with steam gasification of small molecules to produce CO and H_2, followed by CO methanation and CO shift reaction to produce CH_4 and CO_2 (Kong et al., 2008; Sharma et al., 2006).

3.3. Solid product characterisation

3.3.1. Visual observation

From the visual observation, wet hydrochar obtained from reactions at 513 K–533 K were stickier than the wet hydrochar obtained at 493 K and 503 K. The collected hydrochar was placed on an aluminium boat and dried at 378 K for 3 h. The dried hydrochar from experiments 513 K–533 K possessed gummy texture, retaining its sticky and dense consistency, whereas the hydrochar obtained at lower reaction temperature, *viz.* 493 K and 503 K were of powder form.

3.3.2. Proximate & elemental analyses

The proximate analysis was estimated from TGA analysis, as shown in Fig. 6(a) ,(b), (c), (d). The VM, FC, ash content and corresponding HHVs of the POME and hydrochar samples are summarised in Table 3. In comparison to POME, the FC content of the hydrochar increased gradually about 56.69%–63.65%, from 41.47% of the fresh POME), suggesting an increasing conversion of ash-free organic constituents into carbon at higher temperature. Besides, the VM in the hydrochar was significantly lower than that in the fresh POME. Similar findings were reported by Kalderis and co-workers (Kalderis et al., 2014). The decrease of VM content was with the increase in gaseous products when hydrothermal temperature was increased. The ash content showed an increasing uptrend from 7.21% (493 K) to 12.05% (533 K), compared to the fresh POME at 11.54%. The increase of ash content with the elevation of reaction temperature suggests us the decomposition of organic components (Mäkelä and Yoshikawa, 2016).

Table 4 shows the elemental analysis and HHV of freeze-dried fresh POME and hydrochar. Deoxygenation (removal of oxygen from the feed) and the volatile matter conversion (from Table 3) took place, as the oxygen and hydrogen contents were lowered at higher temperature. It is generally accepted that the exothermic reaction which lowers the molecular O/C and H/C ratio is mainly caused by dehydration and decarboxylation (Funke and Ziegler, 2010). This is also in good agreement to the reactions reported by Poerschmann and the team (Poerschmann et al., 2017). The C content of the hydrochar produced was in the range from 55.47% to 66.23% and it was comparable with the C content (20%–78%) of the hydrochar derived from hydrothermal treatment of other compounds (Berge et al., 2011). The elemental C enhancement and diminution of O content suggested improvement of the combustion properties of hydrochar (Khan et al., 2009). Slight amount of N and S elements were detected in the hydrochars.

The rise of elemental C and H and reduction of O content contributes to an increase in HHV value, indicating that the hydrochar is becoming more energy-rich with hydrothermal temperature (Funke and Ziegler, 2010). The HHV of hydrochar is higher than the lignite (16.3 MJ/kg) (Hall, 2012). Hydrochar produced at 533 K showed the highest HHV, which can be attributed to its higher FC and lower VM content. This suggests an energy densification process arising from the solid mass reduction via dehydration and decarboxylation (Kalderis et al., 2014; Danso-Boateng et al., 2013).

3.3.3. SEM-EDX investigation

The SEM-EDX analysis was performed to probe the formation of inorganic salt or chemisorption of nutrients (N, K and P) on the hydrochar. In addition, the effects of different nutrient concentrations on hydrochar formation were analysed. The SEM images of solid hydrochar after 2 h of subcritical hydrothermal processing of POME at 493 K, 513 K

Table 2
Qualitative analysis of major organic compounds via GC-MS.

Organic components	Area (%)					
	Fresh POME	493 K	503 K	513 K	523 K	533 K
Methylamine, N,N-dimethyl-	0.64	0.71	1.18	0.56	0.53	–
1,3-Propanediamine, N,N-dimethyl-	–	1.34	–	–	–	–
Hydrazine, ethyl-	–	6.62	–	–	–	–
Butanoic acid, 3-methyl-	–	–	–	0.74	–	–
Hydrazine, 1,1-dimethyl-	6.54	0.93	0.62	–	–	–
Hydrazine, 1,2-dimethyl-	–	–	0.74	–	–	–
Pentanoic acid	–	0.97	–	1.13	1.98	–
Butanoic acid, 3-methyl-	–	2.13	–	–	–	–
L-Serine, ethyl ester	–	–	3.97	–	–	–
1,2-Ethanediol, diformate	–	–	–	–	2.35	–
Allyl ethyl ether	6.44	–	–	–	–	–
Silacyclopentane	–	0.64	–	–	–	–
Hexanoic acid	–	–	–	–	–	5.43
Butanal, 2-methyl-	–	0.71	–	–	–	–
Pyrrolidine, 1-methyl-	–	–	–	–	0.58	0.84
Pyrrolidin-2-one, 5-[2-butyrylethyl]-	–	–	–	–	3.51	–
2-Hexanone, 4-methyl-	–	0.6	–		–	–
Piperidine, 1-methyl-	–	–	–	–	–	1.01
Thiophene	–	–	–	–	0.63	–
Azetidine, 2,2,3,3-tetramethyl-	–	–	–	–	0.9	–
Aziridine, 2,2,3,3-tetramethyl-	–	–	–	–	–	3.85
1-Buten-3-yne, 2-methyl-	2.35					
N-Ethyl-2-methylallylamine	–	–	–	–	–	0.82
2,2,4,7-Tetramethyl-3,6,9-trioxa-2-silatridecane	–	–	1.34	–	–	–
2-Mercaptothiazole	–	0.75	–	–	–	–
N-t-Butyl-N′-2-[2-thiophosphatoethyl] aminoethylurea	–	–	–	–	–	5.84
2-Octanone	–	–	2.29	–	–	–
5,6-Diamino-1,3-dimethyluracil	–	–	–	0.82	0.6	–
Phenol	–	3.26	–	5.07	3.94	9.01
1,6-Dideoxy-l-mannitol	–	–	–	–	1.97	0.98
1,6-Anhydro-2,4-dideoxy-.beta.-D-ribo-hexopyranose	–	–	–	–	–	1.01
Ethanone, 1-(1H-pyrrol-2-yl)-	–	–	–	–	6.98	3.43
m-Guaiacol		–	–	–	0.78	–
Methanamine, N-methoxy-	1.81	–	–	–	–	–
1,1-Dimethylbutyl (prop-2-enyl)sulfide	–	–	–	–	1.17	–
1-Pentanol, 2,2-dimethyl-	–	–	–	–	–	1.47
O-Methoxy-.alpha.-methylbenzyl alcohol	–	–	–	–	–	1.15
(Z)-4-Methyl-5-(2-oxopropylidene)- 5H-furan-2-one	–	0.52	–	–	–	–
4-Isopropylthiophenol	–	–	–	0.81	–	–
Phenol, 2-(dimethylamino)-	–	–	–	–	–	0.82
Silane, diethoxymethyl-	–	0.92	–	–	–	–
4-Hydroxy-2-methylacetophenone	2.15	–	–	–	–	–
Benzene, 1-isocyano-3-methoxy-	–	2.12	–	–	–	–
Oxime-, methoxy-phenyl-	–	3.29	–	–	–	–
2,3-Dimethylbenzaldoxime	–	21.52	–	–	–	–
4-Ethylbenzoic acid, 2-butyl ester	–	21.36	–	–	–	–
Phenol, 2,6-dimethoxy-	–	–	21.26	23.39	23.93	16.13
1,4-Pentadiene, 2,3,4-trimethyl-	–	1.03	–	–	–	–
6-Acetamido-1,4-benzodioxane	–	3.43	–	–	–	–
Ethanol, 2,2-diethoxy-	–	–	10.21	–	–	–
2,4-Hexadienoyl chloride	–	1.6	–	–	–	–
Cyclohexene, 1-chloro-6-methyl-	–	–	6.43	–	–	–
1H-Indole, 2-methyl-	–	–	–	–	15.95	–
2-Isopropylimidazole	–	–	–	–	13.34	–
1-(1-Propynyl)cyclohexanol	–	–	–	35.89	17.17	40.42
2′,4′-Dihydroxyacetophenone oxime	–	–	0.84	–	–	–
5-tert-Butylpyrogallol	–	–	–	–	1.05	–
1-Methyl-1,6-diazaplenalene	–	–	–	–	–	4.09
Phenol, 2-(dimethylamino)-	1.44	–	–	–	–	–
Hexadecane	–	6.13	–	–	–	–
Phenol, 4-amino-	–	–	–	–	–	1.96
Hexadecanoic acid, methyl ester	–	4.28	23.18	14.38	–	–
Hexadecanoic acid, ethyl ester	–	1.23	–	–	–	–
Heptadecanoic acid, ethyl ester	–	–	–	0.93	–	–
E-11-Tetradecenoic acid	–	–	–	0.55	–	–
n-Hexadecanoic acid	72.58	–	5.14	–	–	–
5-Octadecene, (E)-	1.37					
10-Octadecenoic acid, methyl ester	–	2.23	–	–	–	–
Octadecanoic acid	–	–	–	0.77	–	–
1H-Tetrazol-5-amine	0.92					
cis-13-Octadecenoic acid, methyl ester	–	–	11.36	8.53	–	–
Tetradecanoic acid, 12-methyl-, methyl ester	–	–	0.84	–	–	–

(*continued on next page*)

Table 2 (*continued*)

Organic components	Area (%)					
	Fresh POME	493 K	503 K	513 K	523 K	533 K
Oleic Acid	–	0.6	–	–	–	–
n-Propyl 9-octadecenoate	–	–	–	1.03	–	–
10-Octadecenoic acid, methyl ester	–	–	1.65	–	–	–
N-[Dimethylaminomethyl]aziridine	–	–	0.56	–	–	–
9-Octadecenamide, (Z)-	–	–	0.63	1.03	–	–
Bis(2-ethylhexyl) phthalate	–	0.79	–	–	–	–
Oxazole	1.2	–	–	–	–	–

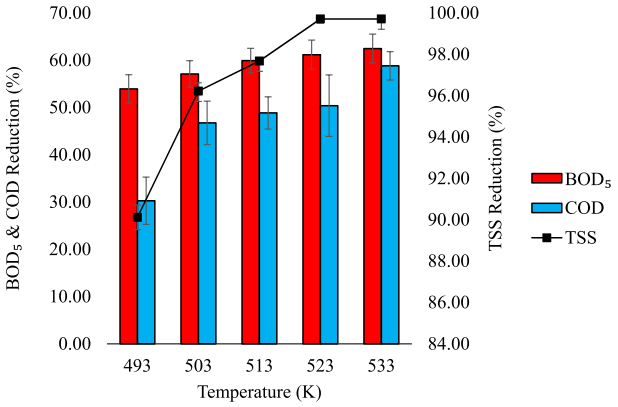

Fig. 2. BOD_5, COD and TSS reduction from 493 K to 533 K.

and 533 K are illustrated in Fig. 7. These hydrochars appeared to be agglomerated and showed insignificant morphological changes. Similar findings were reported previously (Zhu et al., 2015).

Based on EDX analysis, the organic and inorganic compositions of the hydrochar produced through the reaction ranged from 493 K to 533 K are shown in Table 5. Five types of inorganic elements, i.e. Mg, P, K, Ca and Fe, were discovered on the morphological surface of hydrochar. Interestingly, there is no clear correlation pattern between the compositions of inorganic constituents with the reaction temperature, which indicated that hydrothermal reaction only affected the composition of organic compounds. The fluctuation of the composition of inorganic elements with reaction temperature could be due to the degradation of polymeric components, contributing the inorganics from the solid compounds into the liquid (Reza et al., 2014). Table 5 shows that C and O contributed the most in the hydrochar, regardless of the hydrothermal reaction temperature under subcritical condition. The increasing trend of C and reduction of O with the reaction temperature are in good agreement with the elemental analysis.

3.3.4. *O/C & H/C atomic ratios*

The degree of carbonisation was inspected from the aspects of aromaticity using atomic H/C ratio and polarity of the hydrochar by comparing the atomic O/C ratio (Zhu et al., 2015). Both ratios were temperature-dependent (Ma et al., 2016).

Fig. 8 reveals the relationship of atomic O/C and H/C ratios against the reaction temperature. The high O/C and H/C ratios reflect a low degree of aromaticity and a substantial amount of functional groups with elemental O, including hydroxyl, carbonyl, and carboxyl groups (Eibisch et al., 2013). It showed a gradual decrease of O/C atomic ratio when the temperature increased, owing to deoxygenation. The findings were consistent with the proximate analysis. It indicated that the degree of aromatic condensation of hydrochar material increased with the decrease in O/C and H/C atomic ratio (Zhu et al., 2015). A higher degree of aromatic condensation signifies a better stability of hydrochar, contributed by a higher biological resistance and thermochemical degradation (Leng et al., 2019).

Fig. 9 shows the Van Krevelen diagram, a plot that relates the relationship of the O/C atomic and H/C atomic ratios, to characterise natural and derived solid fuels. Fresh POME had comparatively higher atomic O/C and H/C ratios compared to the general biomass. Hydrochar produced at higher reaction temperature had lower atomic O/C and H/C ratios. The hydrochar obtained from hydrothermal reaction of POME exhibited lower O/C and H/C ratios compared to the typical biomass, suggesting it as a potential fuel material.

3.4. *Plausible reaction pathways*

Voluminous studies have been done in hydrothermal treatment (carbonisation, liquefaction and gasification) of model compounds and real biomass. However, a few literature studies focused on the process mechanism of the hydrothermal treatment of wet biomass. Hydrothermal treatment process mechanism to certain extent, is similar to other methods, i.e. pyrolysis, hydrolysis, gasification, but yet it is different from the aforementioned due to the participation of water as the medium, reactant and catalyst (Kong et al., 2008). POME is a wastewater with small amount of suspended solids, giving it a heterogenous identity compared to other kind of wastewater. The interaction of lignocellulosic components in POME due to the oil palm fibrous causing a very complicated chemical mechanism, which cannot be easily summarised (Kong et al., 2008). However, the hydrothermal treatment mechanism can be simplified through a series of simultaneous reactions, including hydrolysis, dehydration, decarboxylation, aromatisation, and recondensation (Libra et al., 2011).

Generally, POME can be decomposed into aqueous and oil product, hydrochar and gaseous products. It is reported that regardless of the feedstock type, four major hydrothermal carbonisation (HTC) reactions occur in this following sequence: (i) dehydration of sugars into furan compounds, (ii) polymerisation or condensation of furan-derivatives, (iii) aromatisation of polymerised products, and (iv) solidification of micromolecules into macromolecules (Reza et al., 2013). For hydrothermal liquefaction (HTL), depolymerisation followed by decomposition and recombination are the possible three major steps take place (Gollakota et al., 2018). (Karagöz et al., 2004) reported that the conversion of biomass increased with the increase of reaction temperature. Hence, it was reasonable that the conversion POME (which exhibits similarly as a wet biomass due to high moisture and lignocellulosic content) is higher with the increase of reaction temperature.

Fig. 10 illustrates the simplified plausible reaction pathways. The tentative pathways of hydrothermal reaction are suggested as following. The autogenous pressure increases with the rise of temperature, causing the cellulose, hemicellulose and lignin components in POME begin to degrade. It is commonly accepted that the acids and alcohols are contributed by the decomposition of cellulose and hemicellulose, while lignin degradation will release phenols and aromatic compounds. At lower temperature, hydrolysis started as the first step to decompose POME into water-soluble products (Williams and Onwudili, 2006). Dehydration and decarboxylation of the hydrolysed components happen simultaneously and instantly after hydrolysis (Reza et al., 2014). During the carbonisation stage, organic compounds in POME decompose to generate organic acids, which would keep the liquid pH lower than 7 and

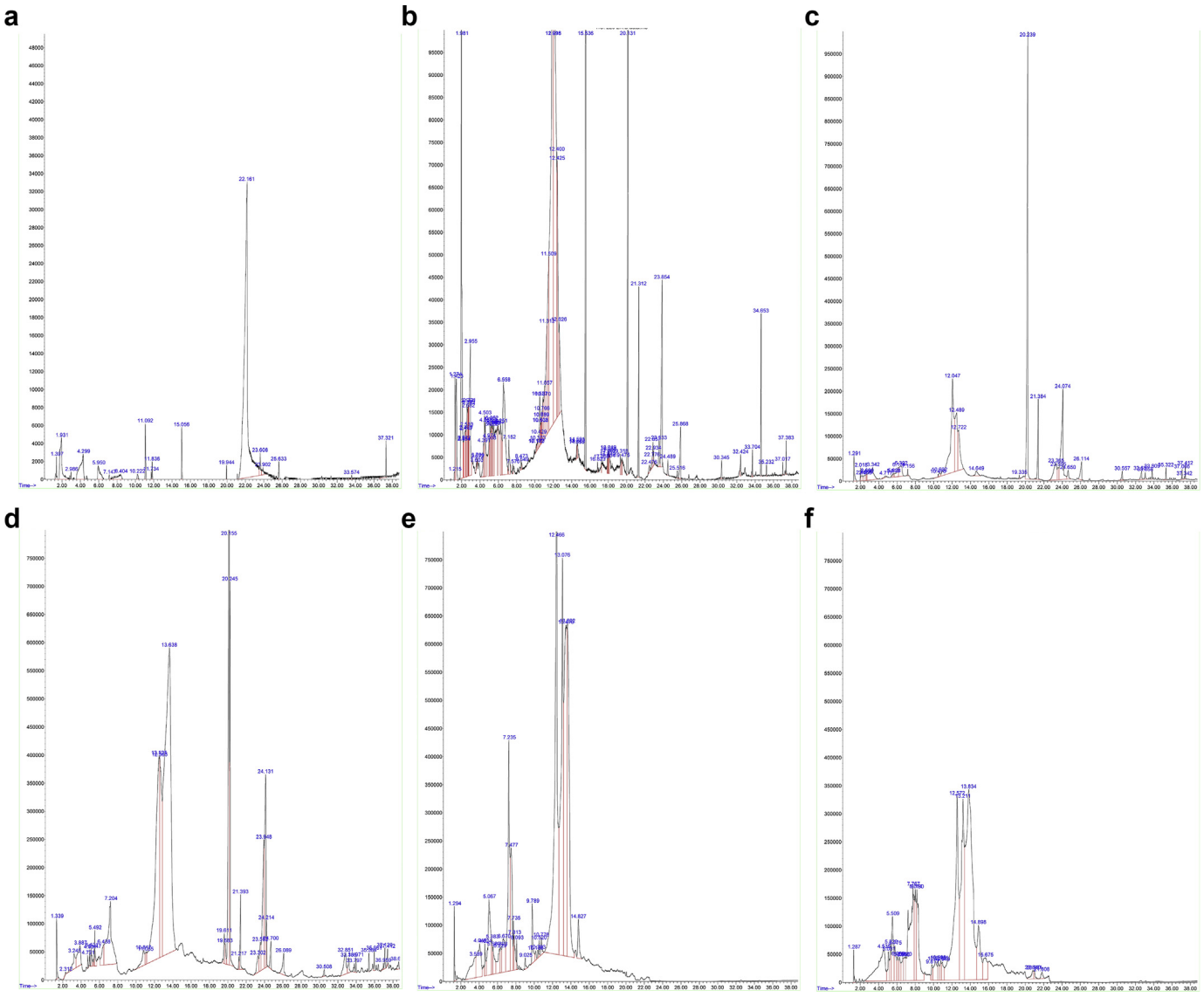

Fig. 3. (a): GC-MS result for freeze-dried fresh POME feed. (b): GC-MS result for freeze-dried liquid product at 493 K. (c): GC-MS result for freeze-dried liquid product at 503 K. (d): GC-MS result for freeze-dried liquid product at 513 K. (e): GC-MS result for freeze-dried liquid product at 523 K. (f): GC-MS result for freeze-dried liquid product at 533 K.

play the role of catalyst in following hydrolysis and decarboxylation reactions (Mäkelä et al., 2018). As the carboxyl compounds decreased with the increase of reaction temperature and plateaued after reaching 523 K, decarboxylation is suggested to happen. This can be explained where the C content increased while O content decreased with the increase of

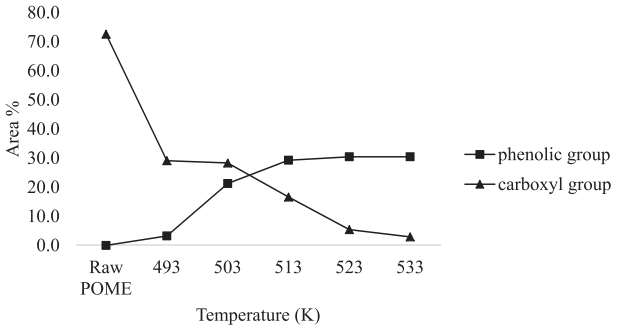

Fig. 4. The variation of phenolic and carboxyl components of fresh POME and liquid products after hydrothermal treatment from 493 K to 533 K.

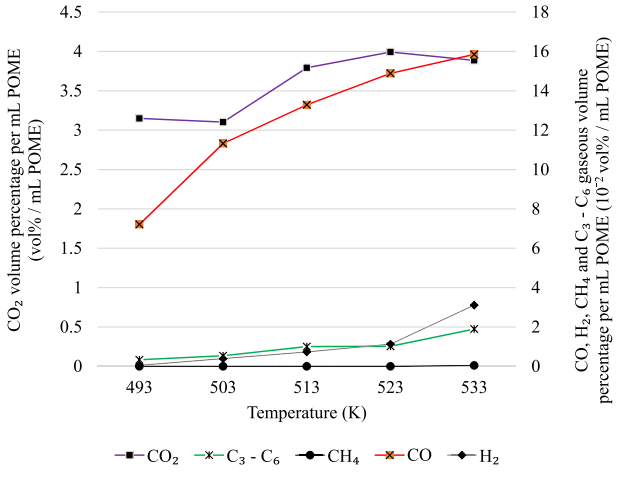

Fig. 5. Composition of gaseous products (vol%/mL POME) in the range of 493 K–533 K.

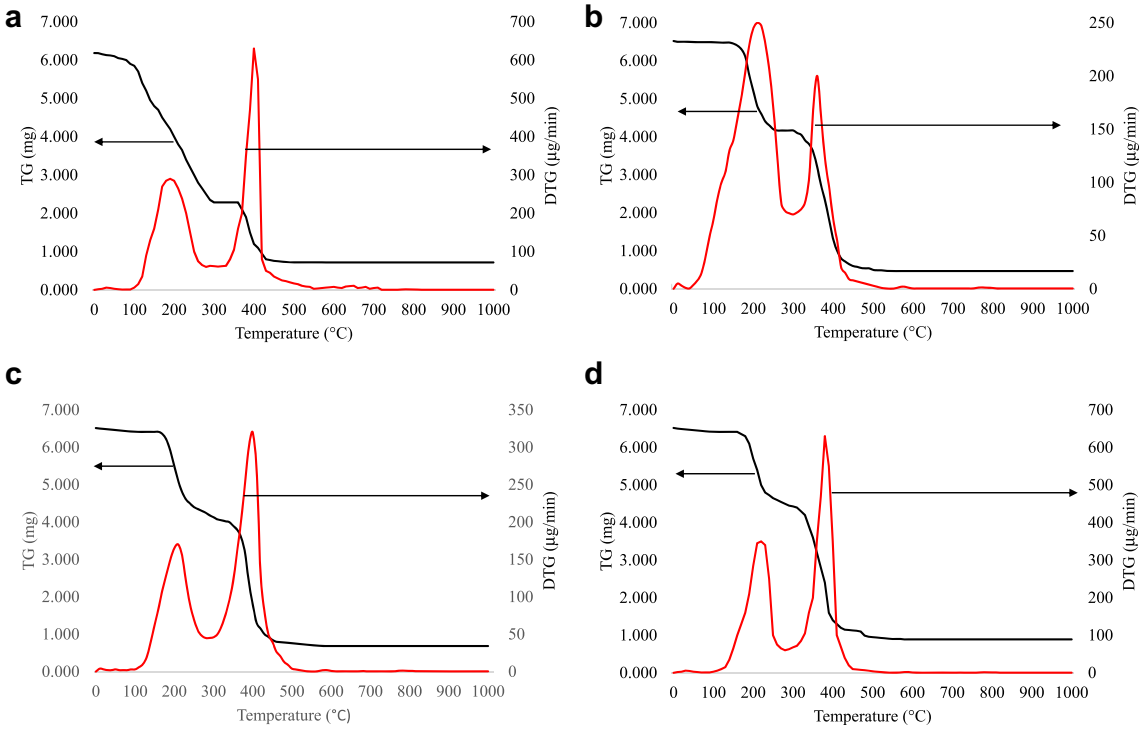

Fig. 6. (a): TGA for freeze-dried fresh POME. (b): TGA for hydrochar at 493 K. (c): TGA for hydrochar at 513 K. (d): TGA for hydrochar at 533 K.

Table 3
Proximate analysis on a dry weight basis of the freeze-dried fresh POME and hydrochar produced at different reaction temperatures.

Sample	VM (%)	FC (%)	Ash Content (%)
Raw POME	46.99	41.47	11.54
493 K	36.10	56.69	7.21
503 K	33.70	57.36	8.94
513 K	30.90	58.60	10.50
523 K	27.40	60.90	11.70
533 K	24.30	63.65	12.05

Table 4
Elemental analysis of freeze-dried fresh POME and hydrochar.

Sample	C (%)	H (%)	N (%)	S (%)	O (%)	HHV (MJ/kg)
Fresh POME	37.358	7.135	2.375	0.979	40.613	17.070
493 K	55.469	6.954	1.143	1.256	27.968	24.624
503 K	58.728	6.552	1.023	1.051	23.706	25.673
513 K	62.474	5.565	1.725	1.700	18.036	26.426
523 K	65.041	5.233	1.946	0.674	15.406	27.072
533 K	66.225	5.128	2.070	0.675	13.852	27.513

process intensity (Zhang et al., 2018). The increase of phenolic compounds indicated the increase of aromatic compounds, suggesting us that dehydration took place (Berge et al., 2011). This is in good agreement with Fig. 9, where the diminution of both atomic H/C and O/C ratios caused by dehydration and decarboxylation. The growth of the aromatic fraction after hydrothermal treatment might probably resulted from the condensation polymerisation (Berge et al., 2011). The reason for the reversible reaction in between acids and phenols where phenols formation was usually the last hindrance to overcome in biomass conversion under hydrothermal treatment (Kong et al., 2008). Based on the gaseous products, CO_2 appeared to be the dominant gas output. It is suggested that the decomposition of the function groups containing oxygen happened (Cheng et al., 2009). The higher concentrations of CO_2 and CO compared to H_2 and CH_4 indicate that the decrease of organic compound in POME during hydrothermal treatment (shown in the result of BOD and COD analyses) is mainly due to decarboxylation and decarbonylation, as well as dehydration reactions (Cheng et al., 2009; Sakaki et al., 1996). A noticeable uptrend of H_2 concentration is observed as the temperature increased from 493 K to 533 K and CH_4 was found only in 533 K, suggesting that the fragmentation of the agricultural fibrous was promoted to some extent at the higher temperature (Cheng et al., 2009). As the ratio of lignin-to-cellulose was high in POME, polymerisation of the lignin compounds was suggested at the range of temperature of 493 K–533 K. Lignin cannot be fully gasified without the formation of solid products at low temperatures (523 K–673 K), due to the presence of recalcitrant phenolic compounds, making polymerisation more favourable compared to decomposition (Kang et al., 2013).

4. Conclusions

Hydrothermal treatment under subcritical condition provides a new idea for the treatment and utilisation of POME. Optimum reaction temperature was at 533 K as it resulted the highest COD, BOD_5 and TSS removal, which recorded at 58.81%, 62.47% and 99.71% respectively, with pH of around 6.5 due to the reduction of carboxylic compounds. Organic compounds with phenolic group increased with reaction temperature. The liquid product wastewater quality is comparable with the effluent in anaerobic section of open ponding system. Further treatment of liquid product, such as aerobic treatment, is recommended as the BOD_5 still has not achieved the local discharge standard. The dominant gaseous product was CO_2, followed by CO, H_2 and higher number hydrocarbons, i.e. C_3 – C_6. CH_4 was found in traces amount at 533 K. Gaseous production increased with the increase of temperature. The FC increased whereas VM reduced in the hydrochar produced at higher temperature. Both the O/C and H/C atomic ratio of the hydrochar produced at 533 K were at the lowest, recorded 0.157 and 0.930 respectively, giving hydrochar a promising behaviour as a combustion fuel. For hydrothermal reaction under subcritical condition, deoxygenation which consisted of dehydration and decarboxylation is proposed to be the major reaction after hydrolysis took place. As POME is richer in lignin, slow

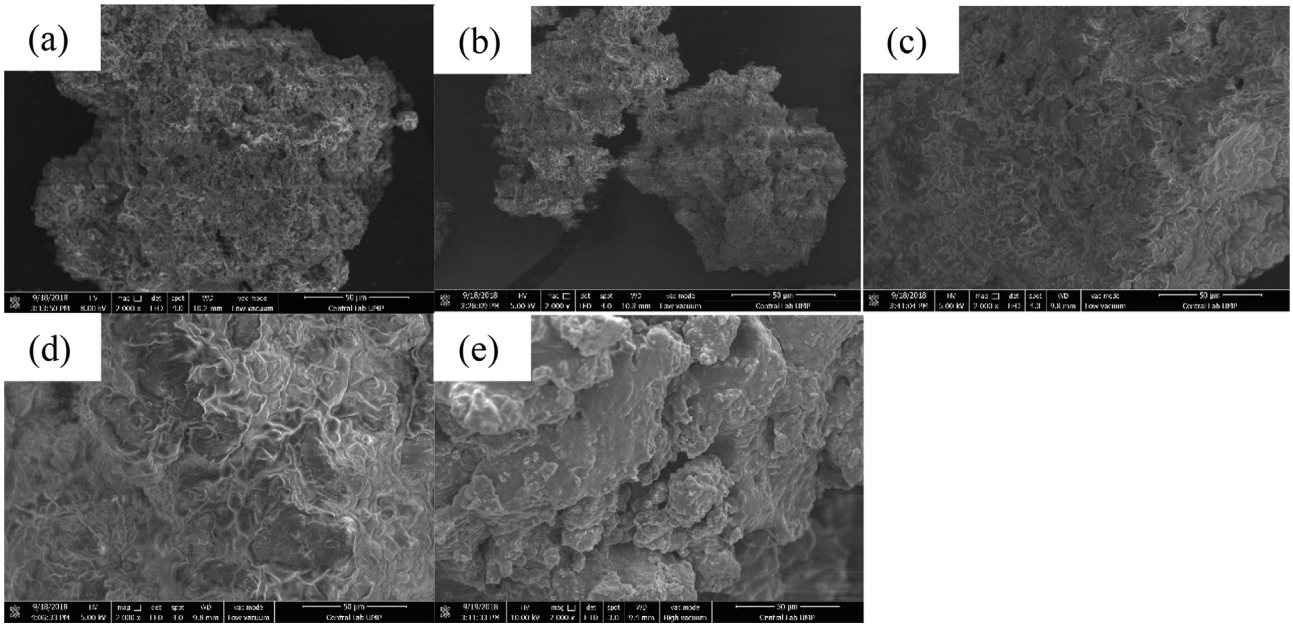

Fig. 7. SEM images of the hydrochar produced at the reaction temperature of (a) 493 K, (b) 503 K, (c) 513 K, (d) 523 K and (e) 533 K.

Table 5
Organic and inorganic composition of hydrochar obtained at various reaction temperature.

Elements	C (%)	O (%)	Mg (%)	P (%)	K (%)	Ca (%)	Fe (%)
493 K	81.656	17.667	0.273	0.039	0.129	0.134	0.102
503 K	82.323	16.712	0.323	0.132	0.218	0.161	0.132
513 K	83.010	15.580	0.299	0.358	0.226	0.336	0.196
523 K	83.430	15.184	0.395	0.373	0.197	0.293	0.123
533 K	84.233	14.541	0.653	0.069	0.196	0.115	0.192

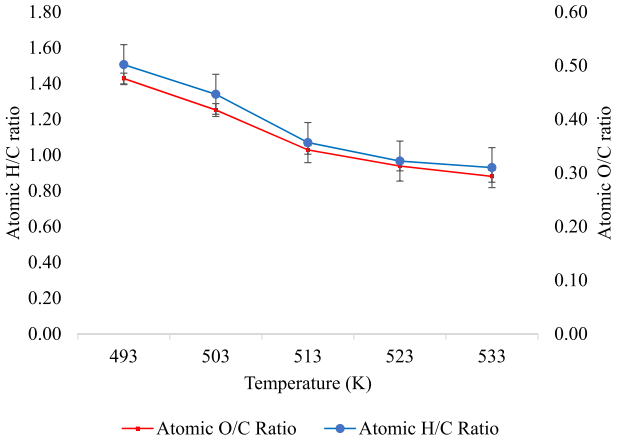

Fig. 8. The atomic H/C and O/C ratios of hydrochar from 493 K to 533 K.

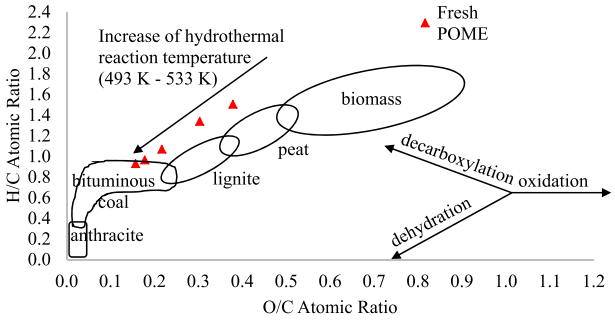

Fig. 9. Van Krevelen diagram.

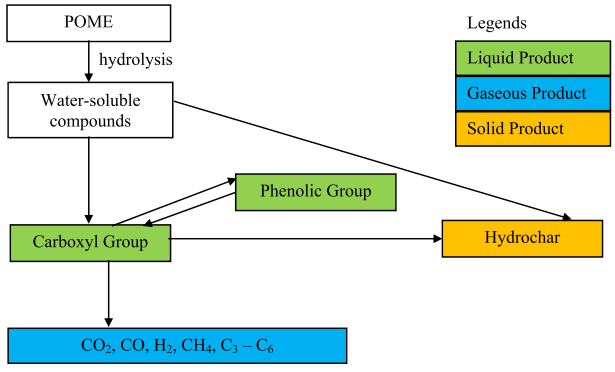

Fig. 10. Plausible reaction pathways of hydrothermal treatment of POME.

polymerisation of lignin into phenolic compounds was suggested with the increase of reaction temperature. Based on the positive treatment output, hydrothermal treatment has a great potentiality to be focused on to overcome the weakness of current open ponding system. A continuous flow study is recommended in future work in order to satisfy the application of this novel POME treatment at elevated scale. One of the industrial concerns of having hydrothermal process for POME treatment will be the plugging problem in continuous flow system. Two-stage hydrothermal treatment (Sintamarean et al., 2017; He et al., 2014) and continuous stirred tank reactor (CSTR) (Ocfemia et al., 2006) are good attempts to overcome the plugging obstacle. In addition, catalytic study is necessary to enhance the organic compounds degradation and to reduce the operation severity. From there, kinetic and process optimisation studies can be performed to deepen the understanding of this novel wastewater treatment.

Declarations

Author contribution statement

Chin Cheng: Conceived and designed the experiments; Analyzed and interpreted the data; Contributed reagents, materials, analysis tools or data.

Zhan Sheng Lee: Performed the experiments; Analyzed and interpreted the data; Contributed reagents, materials, analysis tools or data; Wrote the paper.

Sam Yee Chin: Conceived and designed the experiments; Analyzed and interpreted the data.

Funding statement

This work was supported by UMP Short-Term Grant funding (RDU170325) and also UMP Flagship Strategic Leap 3 Grant (RDU172202). Both grants were awarded by Universiti Malaysia Pahang.

Competing interest statement

The authors declare no conflict of interest.

Additional information

No additional information is available for this paper.

References

Abu Tayeh, H., Levy-Shalev, O., Azaizeh, H., Dosoretz, C.G., 2016. Subcritical hydrothermal pretreatment of olive mill solid waste for biofuel production. Bioresour. Technol. 199, 164–172.

Ahmad, A., Ghufran, R., 2018. Review on industrial wastewater energy sources and carbon emission reduction: towards a clean production. Int. J. Sustain. Eng. 1–11.

Alhaji, M.H., Sanaullah, K., Salleh, S.F., Baini, R., Lim, S.F., Rigit, A.R.H., et al., 2018. Photo-oxidation of pre-treated palm oil mill Effluent using cylindrical column immobilized photoreactor. Process Saf. Environ. Protect.

Ali, A.N.A., Tan, Y.H., Lau, W.J., Lai, G.S., Ong, C.S., Mokhtar, N.M., et al., 2015. Tackling colour issue of anaerobically-treated palm oil mill effluent using membrane technology. J. Water Process Eng. 8, 221–226.

Berge, N.D., Ro, K.S., Mao, J., Flora, J.R.V., Chappell, M.A., Bae, S., 2011. Hydrothermal carbonization of municipal waste streams. Environ. Sci. Technol. 45 (13), 5696–5703.

Chan, Y.J., Tan, W.J.R., How, B.S., Lee, J.J., Lau, V.Y., 2015. Fuzzy optimisation approach on the treatment of palm oil mill effluent (POME) via up-flow anaerobic sludge blanket–hollow centered packed bed (UASB–HCPB) reactor. J. Water Process Eng. 5, 112–117.

Channiwala, S.A., Parikh, P.P., 2002. A unified correlation for estimating HHV of solid, liquid and gaseous fuels. Fuel 81 (8), 1051–1063.

Cheng, J., Zhu, X., Ni, J., Borthwick, A., 2010. Palm oil mill effluent treatment using a two-stage microbial fuel cells system integrated with immobilized biological aerated filters. Bioresour. Technol. 101 (8), 2729–2734.

Cheng, L., Ye, X.P., He, R., Liu, S., 2009. Investigation of rapid conversion of switchgrass in subcritical water. Fuel Process. Technol. 90 (2), 301–311.

Cheng, Y.W., Lee, Z.S., Chong, C.C., Khan, M.R., Cheng, C.K., Ng, K.H., Hossain, S.S., 2018. Hydrogen-rich syngas production via steam reforming of palm oil mill effluent (POME) – a thermodynamics analysis. Int. J. Hydrogen Energy.

Coker, A., 2001. Modeling of Chemical Kinetics and Reactor Design. A.K. Coker.

Danso-Boateng, E., Holdich, R., Shama, G., Wheatley, A.D., Sohail, M., Martin, S., 2013. Kinetics of faecal biomass hydrothermal carbonisation for hydrochar production. Appl. Energy 111, 351–357.

Ding, L., Zou, B., Li, Y., Liu, H., Wang, Z., Zhao, C., et al., 2013. The production of hydrochar-based hierarchical porous carbons for use as electrochemical supercapacitor electrode materials. Colloid. Surf. Physicochem. Eng. Asp. 423, 104–111.

DOSM, D.O.S.M., 2017. Selected Agricultural Indicators. Malaysia, 2017.

Eibisch, N., Helfrich, M., Don, A., Mikutta, R., Kruse, A., Ellerbrock, R., Flessa, H., 2013. Properties and Degradability of Hydrothermal Carbonization Products, vol. 42.

Foong, S.Z.Y., Lam, Y.L., Andiappan, V., Foo, D.C.Y., Ng, D.K.S., 2018. A systematic approach for the synthesis and optimization of palm oil milling processes. Ind. Eng. Chem. Res. 57 (8), 2945–2955.

Funke, A., Ziegler, F., 2010. Hydrothermal carbonization of biomass: a summary and discussion of chemical mechanisms for process engineering. Biofuels, Bioprod. Biorefining 4 (2), 160–177.

Gao, F., Shao, G., Qu, J., Lv, S., Li, Y., Wu, M., 2015. Tailoring of porous and nitrogen-rich carbons derived from hydrochar for high-performance supercapacitor electrodes. Electrochim. Acta 155, 201–208.

Gollakota, A.R.K., Kishore, N., Gu, S., 2018. A review on hydrothermal liquefaction of biomass. Renew. Sustain. Energy Rev. 81, 1378–1392.

Hall, S., 2012. 27 - properties. In: Hall, S. (Ed.), Branan's Rules of Thumb for Chemical Engineers, fifth ed. Butterworth-Heinemann, Oxford, pp. 401–421.

He, C., Chen, C.-L., Giannis, A., Yang, Y., Wang, J.-Y., 2014. Hydrothermal gasification of sewage sludge and model compounds for renewable hydrogen production: a review. Renew. Sustain. Energy Rev. 39, 1127–1142.

Heilmann, S.M., Davis, H.T., Jader, L.R., Lefebvre, P.A., Sadowsky, M.J., Schendel, F.J., et al., 2010. Hydrothermal carbonization of microalgae. Biomass Bioenergy 34 (6), 875–882.

Hosseini, S.E., Wahid, M.A., 2015. Pollutant in palm oil production process. J. Air Waste Manag. Assoc. 65 (7), 773–781.

Islam, M.A., Ahmed, M.J., Khanday, W.A., Asif, M., Hameed, B.H., 2017. Mesoporous activated coconut shell-derived hydrochar prepared via hydrothermal carbonization-NaOH activation for methylene blue adsorption. J. Environ. Manag. 203, 237–244.

Jamal, P., Alam, M.Z., Mohamad, A.B., 2007. Microbial bioconversion of palm oil mill effluent to citric acid with optimum process conditions. In: Paper Presented at the 3rd Kuala Lumpur International Conference on Biomedical Engineering 2006, Berlin, Heidelberg, 2007//.

Kalderis, D., Kotti, M.S., Méndez, A., Gascó, G., 2014. Characterization of hydrochars produced by hydrothermal carbonization of rice husk. Solid Earth 5 (1), 477–483.

Kang, S., Li, X., Fan, J., Chang, J., 2013. Hydrothermal conversion of lignin: a review. Renew. Sustain. Energy Rev. 27, 546–558.

Karagöz, S., Bhaskar, T., Muto, A., Sakata, Y., Uddin, M.A., 2004. Low-temperature hydrothermal treatment of Biomass: effect of reaction parameters on products and boiling point distributions. Energy Fuels 18 (1), 234–241.

Khan, A.A., de Jong, W., Jansens, P.J., Spliethoff, H., 2009. Biomass combustion in fluidized bed boilers: potential problems and remedies. Fuel Process. Technol. 90 (1), 21–50.

Kong, L., Li, G., Zhang, B., He, W., Wang, H., 2008. Hydrogen production from biomass wastes by hydrothermal gasification. Energy Sources, Part A Recovery, Util. Environ. Eff. 30 (13), 1166–1178.

Kruse, A., Funke, A., Titirici, M.-M., 2013. Hydrothermal conversion of biomass to fuels and energetic materials. Curr. Opin. Chem. Biol. 17 (3), 515–521.

Leng, L., Huang, H., Li, H., Li, J., Zhou, W., 2019. Biochar stability assessment methods: a review. Sci. Total Environ. 647, 210–222.

Libra, J.A., Ro, K.S., Kammann, C., Funke, A., Berge, N.D., Neubauer, Y., et al., 2011. Hydrothermal carbonization of biomass residuals: a comparative review of the chemistry, process, and applications of wet and dry pyrolysis. Biofuels 2 (1), 89–124.

Liu, Z., Quek, A., Balasubramanian, R., 2014. Preparation and characterization of fuel pellets from woody biomass, agro-residues and their corresponding hydrochars. Appl. Energy 113, 1315–1322.

Liu, Z., Quek, A., Hoekman, S.K., Balasubramanian, R., 2013. Production of solid biochar fuel from waste biomass by hydrothermal carbonization. Fuel 103, 943–949.

Ma, X., Zhou, B., Budai, A., Jeng, A., Hao, X., Wei, D., et al., 2016. Study of biochar properties by scanning electron microscope – energy dispersive X-ray spectroscopy (SEM-EDX). Commun. Soil Sci. Plant Anal. 47 (5), 593–601.

Mäkelä, M., Forsberg, J., Söderberg, C., Larsson, S.H., Dahl, O., 2018. Process water properties from hydrothermal carbonization of chemical sludge from a pulp and board mill. Bioresour. Technol. 263, 654–659.

Mäkelä, M., Yoshikawa, K., 2016. Part 2: Effects of treatment conditions on industrial waste biomass. Ash Behavior during Hydrothermal Treatment for Solid Fuel Applications, vol. 121.

Montoya, C., Cochard, B., Flori, A., Cros, D., Lopes, R., Cuellar, T., et al., 2014. Genetic architecture of palm oil fatty acid composition in cultivated oil palm (Elaeis guineensis Jacq.) compared to its wild relative E. Oleifera (H.B.K) cortés. PLoS One 9 (5), e95412.

MPOA, 2014. BOD Level and POME Tertiary Treatment Technologies. MPOA News. Retrieved from. http://mpoa.org.my/bod-level-and-pome-tertiary-treatment-technologies/.

MPOB, M.P.O.B., 2017. Monthly Export of Oil Palm Products – 2017.

Nasrullah, M., Singh, L., Mohamad, Z., Norsita, S., Krishnan, S., Wahida, N., Zularisam, A.W., 2017. Treatment of palm oil mill effluent by electrocoagulation with presence of hydrogen peroxide as oxidizing agent and polialuminum chloride as coagulant-aid. Water Resour. Ind. 17, 7–10.

Ng, K., Cheng, C., 2016. Photo-polishing of POME into CH4-lean biogas over the UV-responsive ZnO photocatalyst. Chem. Eng. J. 300, 127–138.

Ng, K.H., Cheng, C.K., 2015. A novel photomineralization of POME over UV-responsive TiO2 photocatalyst: kinetics of POME degradation and gaseous product formations. RSC Adv. 5 (65), 53100–53110.

Ng, K.H., Cheng, Y.W., Lee, Z.S., Cheng, C.K., 2018. A study into syngas production from catalytic steam reforming of palm oil mill effluent (POME): a new treatment approach. Int. J. Hydrogen Energy.

Ng, K.H., Lee, C.H., Khan, M.R., Cheng, C.K., 2016. Photocatalytic degradation of recalcitrant POME waste by using silver doped titania: photokinetics and scavenging studies. Chem. Eng. J. 286, 282–290.

Ocfemia, S.K., Zhang, Y., Funk, T., 2006. Hydrothermal processing of swine manure to oil using a continuous reactor system: effects of operating parameters on oil yield and quality. Trans. ASABE 49 (6), 1897–1904.

Olivier, B., Pierre, F., Bill, C., Keith, P.S., 2009. The indirect global warming potential and global temperature change potential due to methane oxidation. Environ. Res. Lett. 4 (4), 044007.

Osada, M., Sato, T., Watanabe, M., Adschiri, T., Arai, K., 2004. Low-temperature catalytic gasification of lignin and cellulose with a ruthenium catalyst in supercritical water. Energy Fuels 18 (2), 327–333.

Parshetti, G.K., Hoekman, K.S., Balasubramanian, R., 2013. Chemical, structural and combustion characteristics of carbonaceous products obtained by hydrothermal carbonization of palm empty fruit bunches. Bioresour. Technol. 135, 683–689.

Poerschmann, J., Weiner, B., Koehler, R., Kopinke, F.-D., 2017. Hydrothermal carbonization of glucose, fructose, and xylose—identification of organic products with medium molecular masses. ACS Sustain. Chem. Eng. 5 (8), 6420–6428.
Poh, P.E., Chong, M.F., 2009. Development of anaerobic digestion methods for palm oil mill effluent (POME) treatment. Bioresour. Technol. 100 (1), 1–9.
Poh, P.E., Chong, M.F., 2014. Upflow anaerobic sludge blanket-hollow centered packed bed (UASB-HCPB) reactor for thermophilic palm oil mill effluent (POME) treatment. Biomass Bioenergy 67, 231–242.
Reza, M.T., Andert, J., Wirth, B., Busch, D., Pielert, J., Lynam, J., Mumme, J., 2014. Review Article: Hydrothermal Carbonization of Biomass for Energy and Crop Production, vol. 1.
Reza, M.T., Yan, W., Uddin, M.H., Lynam, J.G., Hoekman, S.K., Coronella, C.J., Vásquez, V.R., 2013. Reaction kinetics of hydrothermal carbonization of loblolly pine. Bioresour. Technol. 139, 161–169.
Sakaki, T., Shibata, M., Miki, T., Hirosue, H., Hayashi, N., 1996. Decomposition of cellulose in near-critical water and fermentability of the products. Energy Fuels 10 (3), 684–688.
Salimi, M., Safari, F., Tavasoli, A., Shakeri, A., 2016. Hydrothermal gasification of different agricultural wastes in supercritical water media for hydrogen production: a comparative study. Int. J. Integr. Care 7 (3), 277–285.
Sevilla, M., Fuertes, A.B., 2009. The production of carbon materials by hydrothermal carbonization of cellulose. Carbon 47 (9), 2281–2289.
Sharma, A., Nakagawa, H., Miura, K., 2006. A novel nickel/carbon catalyst for CH4 and H2 production from organic compounds dissolved in wastewater by catalytic hydrothermal gasification. Fuel 85 (2), 179–184.
Simsir, H., Eltugral, N., Karagoz, S., 2017. Hydrothermal carbonization for the preparation of hydrochars from glucose, cellulose, chitin, chitosan and wood chips via low-temperature and their characterization. Bioresour. Technol. 246, 82–87.
Sintamarean, I.M., Grigoras, I.F., Jensen, C.U., Toor, S.S., Pedersen, T.H., Rosendahl, L.A., 2017. Two-stage alkaline hydrothermal liquefaction of wood to biocrude in a continuous bench-scale system. Biomass Convers. Biorefinery 7 (4), 425–435.
Stichnothe, H., Schuchardt, F., 2011. Life cycle assessment of two palm oil production systems. Biomass Bioenergy 35 (9), 3976–3984.
Stirling, R.J., Snape, C.E., Meredith, W., 2018. The impact of hydrothermal carbonisation on the char reactivity of biomass. Fuel Process. Technol. 177, 152–158.
Tabassum, S., Zhang, Y., Zhang, Z., 2015. An integrated method for palm oil mill effluent (POME) treatment for achieving zero liquid discharge – a pilot study. J. Clean. Prod. 95, 148–155.
Takaya, C.A., Fletcher, L.A., Singh, S., Anyikude, K.U., Ross, A.B., 2016. Phosphate and ammonium sorption capacity of biochar and hydrochar from different wastes. Chemosphere 145, 518–527.
Teh, C.Y., Budiman, P.M., Shak, K.P.Y., Wu, T.Y., 2016. Recent advancement of coagulation–flocculation and its application in wastewater treatment. Ind. Eng. Chem. Res. 55 (16), 4363–4389.
Tsai, W.-T., Liu, S.-C., Chen, H.-R., Chang, Y.-M., Tsai, Y.-L., 2012. Textural and chemical properties of swine-manure-derived biochar pertinent to its potential use as a soil amendment. Chemosphere 89 (2), 198–203.
Williams, P.T., Onwudili, J., 2006. Subcritical and supercritical water gasification of cellulose, starch, glucose, and biomass waste. Energy Fuels 20 (3), 1259–1265.
Windeatt, J.H., Ross, A.B., Williams, P.T., Forster, P.M., Nahil, M.A., Singh, S., 2014. Characteristics of biochars from crop residues: potential for carbon sequestration and soil amendment. J. Environ. Manag. 146, 189–197.
Wong, K.M., Nor'aini, A.R., Suraini, A., Vikineswary, S., Hassan, M.A., 2008. Enzymatic hydrolysis of palm oil mill effluent solid using mixed cellulases from locally isolated fungi. Res. J. Microbiol. 3, 474–481.
Wu, Q., Yu, S., Hao, N., Wells, T., Meng, X., Li, M., et al., 2017. Characterization of products from hydrothermal carbonization of pine. Bioresour. Technol. 244 (Pt 1), 78–83.
Wu, T.Y., Mohammad, A.W., Jahim, J.M., Anuar, N., 2010. Pollution control technologies for the treatment of palm oil mill effluent (POME) through end-of-pipe processes. J. Environ. Manag. 91 (7), 1467–1490.
Zahrim, A.Y., Dexter, Z.D., Joseph, C.G., Hilal, N., 2017. Effective coagulation-flocculation treatment of highly polluted palm oil mill biogas plant wastewater using dual coagulants: decolourisation, kinetics and phytotoxicity studies. J. Water Process Eng. 16, 258–269.
Zhang, B., Heidari, M., Regmi, B., Salaudeen, S., Arku, P., Thimmannagari, M., Dutta, A., 2018. Hydrothermal Carbonization of Fruit Wastes: A Promising Technique for Generating Hydrochar, vol. 11.
Zhang, L., Wang, Q., Wang, B., Yang, G., Lucia, L.A., Chen, J., 2015. Hydrothermal carbonization of corncob residues for hydrochar production. Energy Fuels 29 (2), 872–876.
Zhao, M., Li, B., Cai, J.-X., Liu, C., McAdam, K.G., Zhang, K., 2016. Thermal & chemical analyses of hydrothermally derived carbon materials from corn starch. Fuel Process. Technol. 153, 43–49.
Zhu, X., Liu, Y., Qian, F., Zhou, C., Zhang, S., Chen, J., 2015. Role of hydrochar properties on the porosity of hydrochar-based porous carbon for their sustainable application. ACS Sustain. Chem. Eng. 3 (5), 833–840.
Zinatizadeh, A.A.L., Mohamed, A.R., Najafpour, G.D., Hasnain Isa, M., Nasrollahzadeh, H., 2006. Kinetic evaluation of palm oil mill effluent digestion in a high rate up-flow anaerobic sludge fixed film bioreactor. Process Biochem. 41 (5), 1038–1046.